Optical and Electro-Optical Properties of $YbFe_2O_4$ Thin Films

Ram Rai, Josh Hinz, Michelle Pascolini, and Kelly Bryzski

Journal of Nepal Physical Society
Volume 7, No 3, 2021
(Special Issue: ANPA Conference, 2021)
ISSN: 2392-473X (Print), 2738-9537 (Online)

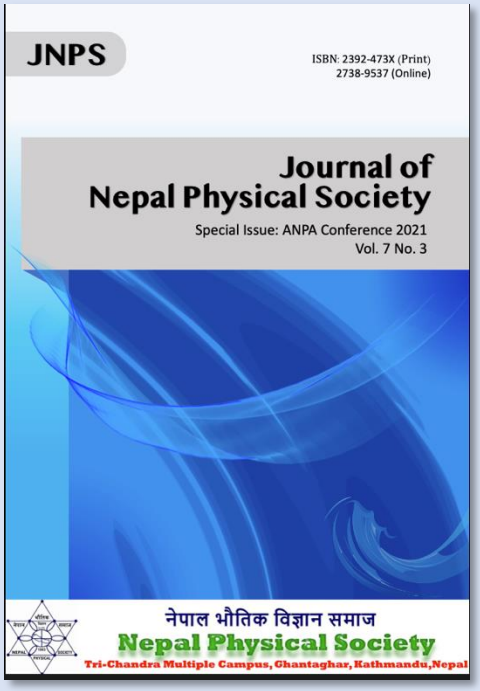

JNPS, **7** (3), 47-52 (2021)
DOI: http://doi.org/10.3126/jnphyssoc.v7i3.42191

Published by: Nepal Physical Society
P.O. Box: 2934
Tri-Chandra Campus
Kathmandu, Nepal
Email: npseditor@gmail.com

ANPA Conference 2021
ISSN:2392-473X (Print), 2738-9537 (Online)

DOI:http://doi.org/10.3126/jnphyssoc.v7i3.42191

Optical and Electro-Optical Properties of $YbFe_2O_4$ Thin Films

Ram Rai[1], Josh Hinz, Michelle Pascolini, and Kelly Bryzski
Department of Physics SUNY Buffalo State,
Buffalo NY 14222 USA
[1)] *Corresponding author: rairc@buffalostate.edu*

Abstract. We present the optical and electro-optical properties of $YbFe_2O_4$ thin films, deposited on (0001) sapphire substrates. The optical spectra of $YbFe_2O_4$ show several electronic peaks arising from Fe^{2+} d to d on-site and O $2p$ to Fe $3d$, Yb $6s$, and Yb $5d$ charge-transfer transitions. The temperature dependence of the d to d electronic transition displays an anomaly around 150 K, which could be associated with a structural instability. Moreover, the $YbFe_2O_4$ thin film show strong electric-field-induced changes in optical properties in the energy range of 1-3 eV for applied electric fields less than 1 kV/cm. These electro-optical effects, which vary almost linearly with applied electric fields, are up to 14 % in magnitude at low temperatures and the effects completely disappear above 120 K. The observed electro-optical effects could be associated with the effects of external electric fields on the orbital-charge ordering of Fe ions.

Received: 14 August 2021; **Revised**: 30 October 2021; **Accepted**: 15 November 2021

Keywords: Thin Films, Multiferroics, Polycrystalline

INTRODUCTION

Materials possessing both magnetic and ferroelectric properties are referred to as multiferroics. These two properties could inter-couple through a unique magneto-electric coupling, making it possible to manipulate the magnetization by electric fields and electric polarization by magnetic fields. Such coupling of the two order parameters is intriguing from the points of view of fundamental physics and potential applications. [1, 2] For example, magnetoelectric coupling is potentially useful for many device applications including magnetic sensors and actuators, storage devices, energy harvesting devices, and spintronic devices. [3, 4, 5, 6, 7, 8] In general, multiferroics are classified into type-I and type-II multiferroics depending on what causes ferroelectrocity in the system. In type-I multiferroices, ferroelectric polarization is caused by one of the physical mechanisms, such as lone-pair electrons, structural distortion, and charge-ordering. [2, 8, 9] The magnetic and ferroelectric orderings occur at two different temperatures and the magnetoelectric coupling is usually weaker. Most of multiferroics discovered so far fall into this category. In type-II multiferroics, a ferroeletric polarization is directly associated with the spin structures that break the inversion symmetry. [2, 8, 9, 10] Because the magnetism induces ferroelectricity, the magnetoelectric coupling is relatively strong in type-II multiferroics but the magnetic transition temperature is well below room temperature. While a tremendous progress has been made in sample synthesis and film fabrication processes, the discovery of room temprature multiferroics with a strong magnetoelectric coupling still remains elusive.

$YbFe_2O_4$ belongs to the RFe_2O_4 (R =Y, Dy to Lu) rare-earth ferrite family which is considered as a multiferroic. [11] This ferrite family has the rhombohedral crystal structure ($R\bar{3}m$) [12] characterized by an alternating stacking of a hexagonal double layer of FeO_5 bipyramids and RO_6 octahedra. Similarly, this family has mixed-valence irons with an equal number of Fe^{2+} and Fe^{3+} ions in a triangular lattice, resulting in both charge and spin frustrations in the system. As a result of the spin and charge frustrations, these ferrites exhibit unique magnetic properties, charge-ordered state, and spin-lattice coupling. [9, 11, 13, 14] The ferrimagnetic transition due to the ordering of the Fe^{2+} and Fe^{3+} moments occurs around 240 K in this family. Similarly, the Fe^{2+} - Fe^{3+} charge-ordered state has been reported in $LuFe_2O_4$ [15, 16, 17] and in $YbFe_2O_4$ [18, 19, 20]. Such charge ordering is believed to break the space-inversion symmetry, leading to macroscopic ferroelectric polarization. [9] This type of ferroelectricity is referred to as electronic ferroelectricity. Furthermore, the structural instability has been reported for $LuFe_2O_4$ and YFe_2O_4. In particular,

the structural distortions from a hexagonal structure to a monoclinic structure and then to a triclinic structure have been reported below the magnetic transition temperature. [21, 22, 23]

While the ferroelectricity driven by the charge ordering mechanism has been proposed for the RFe_2O_4 family, the experimental evidence of a spontaneous polarization in this family is not convincing. For instance, the colossal dielectric properties of $LuFe_2O_4$ and and other RFe_2O_4 members have been associated with ferroelectricity. [11, 24, 25, 26] In contrary, the colossal dielectric property of $LuFe_2O_4$ is controversial because the dielectric data can be described by the extrinsic effects, such as the Maxwell-Wagner model. [27, 28, 29, 30, 31] On the other hand, recently Nagata et. al have reported the spontaneous electric polarization in $YbFe_2O_4$. [32] Similarly, Fujiwara et. al have used second harmonic generation and neutron diffraction to confirm the existence of electronic ferroelectricity in $YbFe_2O_4$. [33] These new reports certainly bring attention to the electronic ferroelectricity in $YbFe_2O_4$. Although there has been a decent amount of work on $YbFe_2O_4$, most of the published articles have been on the bulk samples and there is only a small number of studies on $YbFe_2O_4$ thin films. [34, 35, 36, 37] Additionally, the systematic studies on the optical properties and electronic excitations of $YbFe_2O_4$ are very limited. Since both ferroelectric and magnetic properties of $YbFe_2O_4$ come from the Fe *d* electrons, understanding of the electronic transitions and their temperature dependence is very important. And, for such studies, $YbFe_2O_4$ thin films are well suited than the bulk samples. Moreover, the electro-optical effects of the ferrite family could offer insight into the charge-ordered state and possible existence of ferroelectricity. We can utilize optical spectroscopy to investigate the optical and electro-optical properties of $YbFe_2O_4$.

In this article, we report on the optical and electro-optical properties of $YbFe_2O_4$ thin films, deposited on (0001) sapphire substrates by a reactive electron beam deposition system. We measured the temperature-dependent optical spectra in the temperature range of 10 - 300 K using optical spectroscopy. We show that the optical spectra of $YbFe_2O_4$ manifest several electronic transitions attributed to Fe^{2+} d to d on-site and O $2p$ to Fe $3d$, Yb $6s$, and Yb $5d$ charge-transfer transitions. The temperature dependent absorption data shows a subtle change around $\sim$150 K. The electro-optical properties of $YbFe_2O_4$ have been measured and discussed in the context of a ferroelectric state in the system.

EXPERIMENTAL METHODS

$YbFe_2O_4$ was prepared by a conventional solid state reaction. The powder samples ($\sim$99.9% purity from Alfa Aesar Inc.) of Yb_2O_3, Fe_2O_3, and FeO were mixed in a stoichiometric ratio. The mixture was thoroughly ground in mortal and pestal and then pressed into pellets and sintered at 1100 °C for 15 hours in a tube furnace. After sintering, the process was repeated two more times: ground, pressed into pellets, and sintered. Finally, the prepared pellets (13 mm x 5 mm) were used as a target material for the electron beam deposition. Before film deposition, we preheated substrates to 600 °C and maintained at this temperature for 30 min to remove any residues from the substrates. Then, we slowly increased the substrate temperature to the final temperature (830 °C). As for the source target, we slowly and carefully increased the electron beam power so that the pellet surface started melting without spattering of the material. Once the target surface started melting, the film deposition rate increased significantly. Controlling of the power is the key to the quality of the thin films. We deposited thicker than 100 nm $YbFe_2O_4$ films on single crystal (0001) sapphire and (111) yttrium-stabilized zirconia substrates, maintained at 830 °C with the film deposition rate of 90 Å/min. The film thickness was measured by a quartz crystal monitor during the deposition process and later by an optical method. The chamber base pressure and the oxygen partial pressure were 2.5 x 10^{-4} Pa and 5 x 10^{-2} Pa, respectively. All deposited thin films were annealed at 600 °C in the mixture of oxygen and air for about 3 hours.

We measured variable-temperature (10 - 300 K) normal-incidence optical transmittance and reflectance in the wavelength range of 190 - 2500 nm, with a spectral resolution of 1 nm, using a dual-beam spectrophotometer (Lambda 950, Perkin Elmer) and in the wavelength range of 250 - 1000 nm, with a spectral resolution of 1 nm, using a fiber optic spectrometer (StellarNet) coupled with a closed-cycle helium refrigeration system. For the electro-optical measurements, gold films were evaporated on the two sides of the sample and the copper wires were attached with silver paste [as shown in the inset of Fig. 4(b)]. The thin film length was about $\sim$3-4 mm long between the electrodes. The electric fields were applied to the sample using a Keithley 2400 source meter. All electro-optical measurements were carried out by the fiber optic spectrometer with a charge-coupled detector (2048 pixel). The integration time for the detector was used between 1 and 2 seconds, thus minimizing any possible sample heating due to Joule heating as well as a signal drifting issues.

RESULTS AND DISCUSSION

We present below the optical and electro-optical data of the polycrystalline $YbFe_2O_4$ thin films, deposited by a reactive electron-beam evaporation. The thin film characterizations have been presented elsewhere. [38] We car-

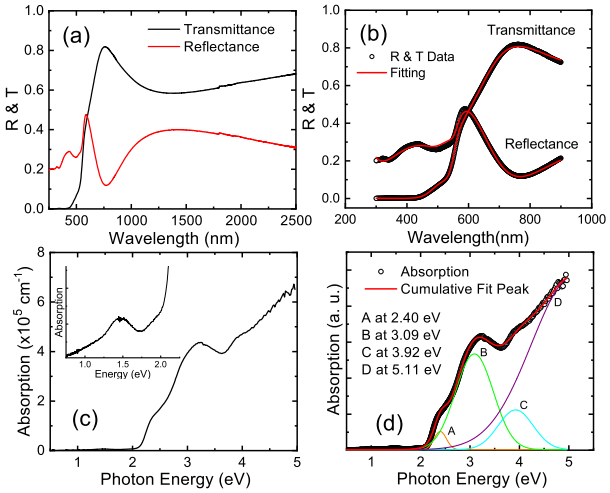

FIGURE 1. (a) Room temperature reflectance and transmittance as a function of wavelength for a $YbFe_2O_4$/sapphire film. (b) The simultaneous fitting of the reflectance and transmittance data using the fitting model [39, 40, 41] to estimate the thickness of the film which was estimated to be ∼145 nm. (c) The absorption coefficient (α) of the $YbFe_2O_4$ film at 300 K, extracted from the measured transmittance and reflectance. The inset shows a close-up view of a very weak peak centered around ∼1.5 eV. (d) The peak fitting of the absorption spectrum. A solid line (red) represents the fitting for the absorption (solid circle) with 4 peaks as indicated by the colored solid lines. The Gaussian function was used for the peak fitting process.

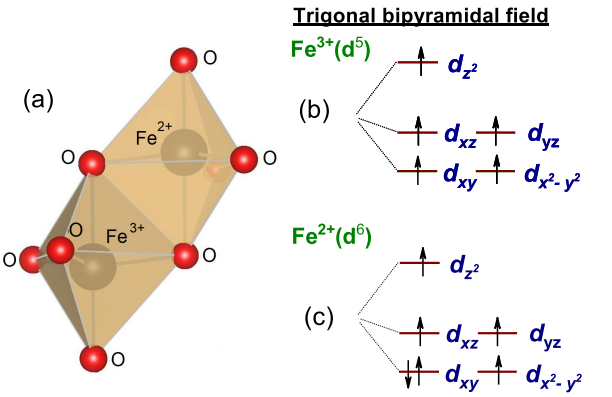

FIGURE 2. (a) FeO_5 trigonal bipyramids are the building block of the $YbFe_2O_4$ structure. Two bipyramids with Fe^{3+} and Fe^{2+} ions, respectively, at the center of the bipyramids are shown. The crystal-field splitting of (b) $Fe^{3+}(d^5)$ and (c) $Fe^{2+}(d^6)$ due to the oxygen ligands. The arrows represent the d-electrons with their spins in each state.

ried out the transmittance and reflectance measurements on multiple $YbFe_2O_4$/sapphire thin films with zero field and with applied electric fields in order to investigate the absorption spectrum and electro-optical properties.

Figure 1(a) shows the room temperature reflectance (R) and transmittance (T) spectra for a $YbFe_2O_4$/sapphire thin film. The reflectance and transmittance spectra were simultaneously fitted to measure the thickness of the film. [39, 40, 41] We used the TFCompanion software (Semiconsoft Inc.) to fit the spectra, as shown in Fig. 1(b). The fits compare reasonably well with the experimental data. The solid lines represent the fittings, and the thickness of the film was measured to be ∼145 ± 5 nm. Room temperature absorption coefficient (α) versus photon energy for $YbFe_2O_4$ is shown in Fig. 1 (c). The absorption coefficient was calculated using $\alpha = -(1/d)ln[T/(1-R)]$, where d is the film thickness, R is the reflectance, and T is the transmittance. The inset shows a close-up view of the low energy region, highlighting the presence of an extremely weak electronic transition. In order to identify the energies of the electronic transitions, the absorption spectrum was fitted with the Gaussian-amplitude function. The best fit (red solid line) was obtained with 4 peaks at ∼2.40, 3.09, 3.92, and 5.11 eV, as indicated by the color solid lines. These four peaks are labeled as A, B, C, and D, respectively. Because the peak centered around 1.5 eV is extremely weak, we decided not to include it in the fitting process.

Optical spectroscopy in the visible and ultra-violate energy range can capture the intra-atomic and inter-atomic electronic transitions in most complex oxides. Here, the absorption spectrum of $YbFe_2O_4$ contains five electronic excitations, including the weak peak at 1.5 eV. The absorption spectrum is very similar to that of isostructural $LuFe_2O_4$ and YFe_2O_4 thin films. [42, 43] Based on the first principle calculations [44, 45] and the optical data [46], we assigned the peaks near ∼1.50 eV and ∼2.40 eV to the Fe^{2+} ($3d^6$) d to d electronic transitions. Weak oscillator strengths of these transitions are consistent with the fact that these Fe d to d transitions are normally forbidden by the Laporte rule, but the p-d hybridization, the local distortion and/or the spin-lattice coupling in the system relax the selection rules. The broad transitions centered at 3.09 eV, 3.92 eV, and 5.11 eV are mainly due to the O $2p$ to Fe $3d$, Yb $6s$ and $5d$ charge-transfer electronic transitions.

Figure 2(a) shows the two FeO_5 trigonal bipyramids which are the building block of the $YbFe_2O_4$ structure. The center of these bipyramids are occupied by two different Fe ions. One bipyramid has Fe^{3+} and the other has Fe^{2+} at the center. The crystal-field splitting of the Fe $3d$ orbitals in the FeO_5 trigonal bipyramidal environment are shown in Fig. 2 (b) and (c). The five-coordinated oxygen ligand fields in FeO_5 split the originally degenerated Fe d states into three groups: (d_{xy}, $d_{x^2-y^2}$), (d_{xz}, d_{yz}), and d_{z^2}. [44, 45] Since the $Fe^{2+}(d^6)$ ions are in a high spin state, all five d-states are singly occupied except the lowest one which is doubly occupied by two electrons with anti-parallel spins (up and down arrows). For $Fe^{3+}(d^5)$

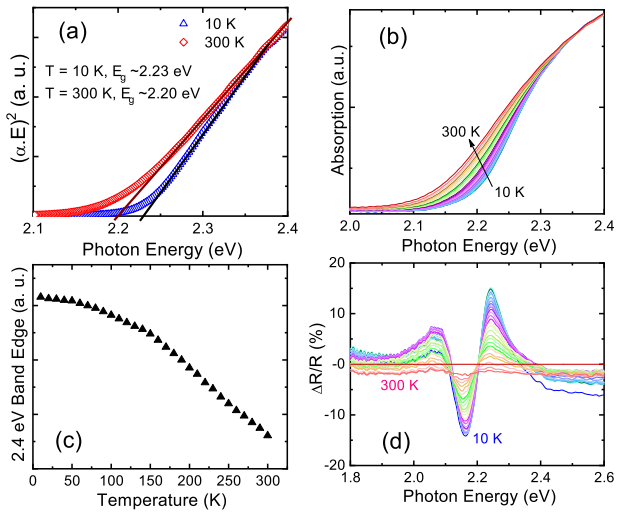

FIGURE 3. (a) The energy bandgap extraction from the $(\alpha \cdot E)^2$ versus photon energy for $YbFe_2O_4$ at 10 K and 300 K, respectively. A solid line represents the fitting of the graph using the direct energy band gap model. (b) A close-up view of the absorption spectra in the low-energy region between 10 and 300 K. (c) Temperature dependence of the absorption edge of the 2.40 eV electronic transition, indicating a non-linear behavior. (d) The reflectance ratio [ΔR(T)/R] as a function of photon energy between 10 K and 300 K. The reflectance at each temperature (in a temperature increment of 10 K) is divided by the 300 K reflectance data.

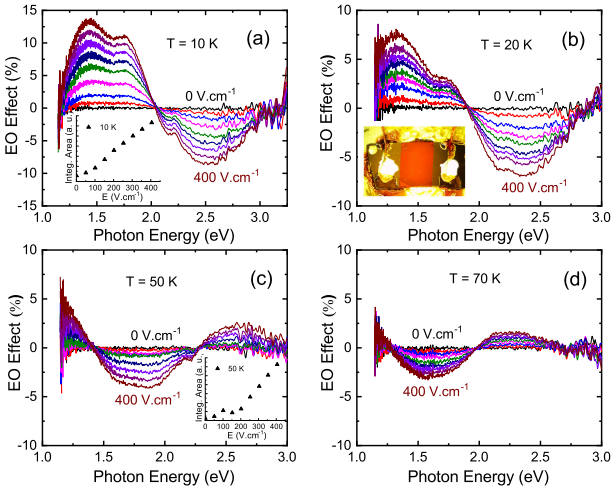

FIGURE 4. The electro-optical response [ΔR(E)/R] of a $YbFe_2O_4$ thin film as a function of photon energy at (a) 10 K, (b) 20 K, (c) 50 K, and (d) 70 K, respectively. The EO effects are up to $\geq$10 % at 10 K and ±3 % at 70 K. The integrated area of the EO effects at 10 K and 50 K varies linearly with the applied electric fields, as shown in the insets of (a) and (c). The EO effects are localized in the 1.25 - 3.0 eV range. The inset of (b) shows the sample with copper wires mounted on the gold electrodes.

ions, all five d-states are singly occupied. Therefore, with the given electronic configurations, there are two possible spin-allowed electronic transitions in $Fe^{2+}(d^6)$: $d_{xy} \rightarrow (d_{xz}, d_{yz})$, and $d_{xy} \rightarrow d_{z^2}$, which are consistent with the observed electronic transitions at 1.50 and 2.40 eV in the absorption spectrum. On the other hand, there are no spin-allowed electronic transitions in $Fe^{3+}(d^5)$ because each d-state is only singly occupied by five electrons.

The energy bandgap of the $YbFe_2O_4$ thin film can be extracted by fitting the $(\alpha \cdot E)^2$ versus energy (E) data to the theoretical model, $\alpha(E) = \frac{A}{E}(E - E_g)^{\frac{1}{2}}$ [47], where E_g is the direct energy band gap and A is a constant. Figure 3(a) shows the $(\alpha \cdot E)^2$ versus E graphs for $YbFe_2O_4$ at 10 K and 300 K, respectively. The solid lines represent the fitting of the graph using the direct energy band gap model. The energy bandgaps were measured to be 2.20 $\pm$ 0.03 eV and 2.23 $\pm$ 0.03 eV at 300 K and 10 K, respectively. Figure 3(b) shows a close-up view of the low-energy region of the absorption spectra between 10 and 300 K. The band edge shifts to the higher energy region on cooling. To study the temperature dependence, we extracted the absorption edge of the 2.40 eV electronic transition for each temperature. We measured the intensity of the absorption edge at 2.20 eV, as shown in Fig. 3(c), which displays a non-linear behavior. The slope of the the curve changes below 150 K, suggesting that the electronic structures are different below and above 150 K. It is very likely that this non-linear behavior of the absorption edge is indicative of the low temperature structural changes below 170 K. We earlier reported the non-linear temperature dependence of the energy gap for $YbFe_2O_4$. [38] Figure 3(d) shows the reflectance ratio [ΔR(T)/R] as a function of photon energy between 10 K and 300 K. The reflectance at each temperature is divided by the 300 K reflectance data. We discuss this graph in relation to the electro-optical effects below.

In order to investigate the electric-field induced changes in the optical properties, we measured the electro-optical effects [ΔR/R = R(E)/R(0)-1] of a $YbFe_2O_4$ thin film. Here, R is the reflectance of the sample and E is the applied electric field on the sample. Figure 4 (a-d) shows the electro-optical (EO) response of the $YbFe_2O_4$ thin film as a function of photon energy at 10 K, 20 K, 50 K, and 70 K, respectively. The electric field was applied in an increment of 50 V/cm and the maximum field was 400 V/cm. The inset of Fig. 4b shows a typical sample with gold films and copper wires mounted on the sample to apply the electric fields. The observed EO effects were the largest, up to 14 %, at 10 K. The EO responses decreased at higher temperatures. For example, the EO effects for E = 400 V/cm were $\sim$8 % at 20 K, $\sim$5 % at 50 K, and $\sim$3 % at 70 K. The EO responses completely disappear around 120 K.

We compare the EO effects with the temperature induced changes in the reflectance (Fig. 3d) to understand

if a sudden change in the sample temperature contributes to the observed EO effects. It is noted that a typical resistance of a $YbFe_2O_4$ thin film is on the order of 10^{12} Ω below 100 K, which means that the Joule heating effect on the sample for E = 400 V/cm would be very small. Further, we note that the sample is being continuously cooled while taking the data and the data acquisition time was less than 2 seconds. One of the main reasons we carried out the EO measurements using a fiber optic spectrometer was that the spectrometer has a charge-coupled detector which enables us to capture the whole spectrum (250 - 1080 nm) within a few seconds, thus minimizing any sample heating issues. As shown in Fig. 3d, the temperature induced effects (ΔR/R) are 1-2 % for a temperature change of ∼10 K and about 15 % for a temperature change of ∼290 K. Even if the sample temperature was increased due to Joule heating, it would be on the order of 10 K. Consequently, the contributions of the heating effects on the observed EO effects are insignificant. Moreover, the temperature-induced ΔR/R is mostly localized between 2 eV and 2.5 eV whereas the EO effects are spread over the 1.25 - 3 eV range, indicating that the EO effects are indeed the field-induced effects.

For the given temperature, the EO effect increases with the applied field. To understand the field dependence of the effects, we integrated the area under the EO curve for each field. The insets of Fig. 4(a),(c) show the integrated area of the EO effects as a function of E for 10 and 50 K. As shown, the EO effects vary almost linearly with the applied electric fields, confirming that the EO effects are linear in $YbFe_2O_4$. Note that the EO effects are mostly observed between ∼1.25 and 3.0 eV where Fe d to d on-site electronic transitions take place. Moreover, the Fe^{2+} and Fe^{3+} ions are reported to have the orbital-charge ordering in $YbFe_2O_4$. [9, 11] Therefore, the observed EO effects can be linked with the effects of external electric fields on the orbital-charge ordering of the Fe ions, consequently affecting the Fe d to d transitions. We have observed similar but weaker EO effects in isostructural YFe_2O_4 and $LuFe_2O_4$ thin films. [42, 43] It is likely that the EO effects in the RFe_2O_4 family are the results of the Fe^{2+}- Fe^{3+} orbital-charge orderings and therefore, the EO effects could have a direct link with ferroelectricity in RFe_2O_4. Our future work will focus on understanding the charge-ordering induced ferroelectricity and its connections with the EO effects in the RFe_2O_4 system.

CONCLUSION

In summary, we investigated the optical absorption, electronic excitations, and EO effects in the polycrystalline $YbFe_2O_4$ thin films. The absorption spectrum of $YbFe_2O_4$ show two Fe d to d on-site transitions at 1.50 eV and 2.40 eV, while the charge-transfer transitions from O $2p$ to Fe $3d$, Yb $6s$, and Yb $5d$ are observed at 3.09 eV, 3.92 eV, and 5.11 eV, respectively. And, these electronic transition display strong temperature dependence with an anomaly at ∼150 K, indicating a structural instability. More importantly, $YbFe_2O_4$ exhibits strong electric-field-induced changes in optical properties in the 1-3 eV energy range for applied electric fields up to 400 V/cm. The linear EO effects are greater than 10 % at low temperatures which completely disappear at ∼120 K. The observed EO effects are caused by the effects of external electric fields on the Fe^{2+}- Fe^{3+} orbital-charge ordering. Finally, the EO effects and ferroelectricity could possibly be directly related in $YbFe_2O_4$.

ACKNOWLEDGMENTS

Work at SUNY Buffalo State was supported by SUNY Buffalo State's Office of Undergraduate Research and the National Science Foundation (DMR-1406766).

EDITOR'S NOTE

This manuscript was submitted to the Association of Nepali Physicists in America (ANPA) Conference 2021 for publication in the special issue of Journal of Nepal Physical Society.

REFERENCES

1. R. Ramesh and N. A. Spaldin, "Multiferroics: progress and prospects in thin films," Nanoscience And Technology: A Collection of Reviews from Nature Journals , 20–28 (2010).
2. N. A. Spaldin, "Multiferroics: Past, present, and future," MRS Bulletin **42**, 385–390 (2017).
3. J. F. Scott, "Room-temperature multiferroic magnetoelectrics," NPG Asia Materials **5**, e72–e72 (2013).
4. M. M. Vopson, "Fundamentals of multiferroic materials and their possible applications," Critical Reviews in Solid State and Materials Sciences **40**, 223–250 (2015).
5. N. Ortega, A. Kumar, J. Scott, and R. S. Katiyar, "Multifunctional magnetoelectric materials for device applications," Journal of Physics: Condensed Matter **27**, 504002 (2015).
6. T. Jia, Z. Cheng, H. Zhao, and H. Kimura, "Domain switching in single-phase multiferroics," Applied Physics Reviews **5**, 021102 (2018).
7. J.-M. Hu and C.-W. Nan, "Opportunities and challenges for magnetoelectric devices," APL Materials **7**, 080905 (2019).
8. C. Lu, M. Wu, L. Lin, and J.-M. Liu, "Single-phase multiferroics: new materials, phenomena, and physics," National Science Review **6**, 653–668 (2019).
9. J. van den Brink and D. I. Khomskii, "Multiferroicity due to charge ordering," Journal of Physics: Condensed Matter **20**, 434217 (2008).
10. S. Dong, H. Xiang, and E. Dagotto, "Magnetoelectricity in multiferroics: a theoretical perspective," National Science Review **6**, 629–641 (2019).

11. N. Ikeda, H. Ohsumi, K. Ohwada, K. Ishii, T. Inami, K. Kakurai, Y. Murakami, K. Yoshii, S. Mori, Y. Horibe, *et al.*, "Ferroelectricity from iron valence ordering in the charge-frustrated system $LuFe_2O_4$," Nature **436**, 1136–1138 (2005).
12. K. Kato, I. Kawada, N. Kimizuka, and T. Katsura, "Die kristallstruktur von $YbFe_2O_4$," Zeitschrift für Kristallographie **141**, 314–320 (1975).
13. A. Nagano, M. Naka, J. Nasu, and S. Ishihara, "Electric polarization, magnetoelectric effect, and orbital state of a layered iron oxide with frustrated geometry," Phys. Rev. Lett. **99**, 217202 (2007).
14. M. Naka, A. Nagano, and S. Ishihara, "Magnetodielectric phenomena in a charge- and spin-frustrated system of layered iron oxide," Phys. Rev. B **77**, 224441 (2008).
15. F. Sun, R. Wang, C. Aku-Leh, H. Yang, R. He, and J. Zhao, "Double charge ordering states and spin ordering state observed in a RFe_2O_4 system," Scientific Reports **4**, 1–5 (2014).
16. D. Kim, J. Hwang, E. Lee, J. Kim, B. Lee, H.-K. Lee, J.-Y. Kim, S. Han, S. Hong, C.-J. Kang, *et al.*, "Interplay between R 4f and Fe 3d states in charge-ordered RFe_2O_4 (R= Er, Tm, Lu)," Physical Review B **87**, 184409 (2013).
17. I. Yang, J. Kim, S. Lee, S.-W. Cheong, and Y. Jeong, "Charge ordering, ferroelectric, and magnetic domains in $LuFe_2O_4$ observed by scanning probe microscopy," Applied Physics Letters **106**, 152902 (2015).
18. H. Williamson, T. Mueller, M. Angst, and G. Balakrishnan, "Growth of $YbFe_2O_4$ single crystals exhibiting long-range charge order via the optical floating zone method," Journal of Crystal Growth **475**, 44–48 (2017).
19. Y. Murakami, N. Abe, T. Arima, and D. Shindo, "Charge-ordered domain structure in $YbFe_2O_4$ observed by energy-filtered transmission electron microscopy," Physical Review B **76**, 024109 (2007).
20. H. Kobayashi, K. Fujiwara, N. Kobayashi, T. Ogawa, M. Sakai, M. Tsujimoto, O. Seri, S. Mori, and N. Ikeda, "Stability of cluster glass state in nano order sized $YbFe_2O_4$ powders," Journal of Physics and Chemistry of Solids **103**, 103–108 (2017).
21. S. Lafuerza, J. García, G. Subías, J. Blasco, and V. Cuartero, "Strong local lattice instability in hexagonal ferrites RFe_2O_4 (R= Lu, Y, Yb) revealed by x-ray absorption spectroscopy," Physical Review B **89**, 045129 (2014).
22. N. Ikeda, T. Nagata, J. Kano, and S. Mori, "Present status of the experimental aspect of RFe_2O_4 study," Journal of Physics: Condensed Matter **27**, 053201 (2015).
23. M. Tanaka, J. Akimitsu, Y. Inada, N. Kimizuka, I. Shindo, and K. Siratori, "Conductivity and specific heat anomalies at the low temperature transition in the stoichiometric YFe_2O_4," Solid State Communications **44**, 687–690 (1982).
24. C. Li, X. Zhang, Z. Cheng, and Y. Sun, "Electric field induced phase transition in charge-ordered $LuFe_2O_4$," Applied Physics Letters **93**, 152103 (2008).
25. Y. Hou, Y. Yao, S. Dong, X. Huang, X. Sun, and X. Li, "Tunable dielectric properties in mn-doped $LuFe_2O_4$ system," Journal of Materials Research **27**, 922–927 (2012).
26. M. Zeng, J. Liu, Y. Qin, H. Yang, J. Li, and J. Dai, "Dielectric tunability and magnetoelectric coupling in $LuFe_2O_4$ epitaxial thin film deposited by pulsed-laser deposition," Thin Solid Films **520**, 6446–6449 (2012).
27. J. d. de Groot, T. Mueller, R. Rosenberg, D. Keavney, Z. Islam, J.-W. Kim, and M. Angst, "Charge order in $LuFe_2O_4$: an unlikely route to ferroelectricity," Physical Review Letters **108**, 187601 (2012).
28. P. Ren, Z. Yang, W. Zhu, C. Huan, and L. Wang, "Origin of the colossal dielectric permittivity and magnetocapacitance in $LuFe_2O_4$," Journal of Applied Physics **109**, 074109 (2011).
29. D. Niermann, F. Waschkowski, J. de Groot, M. Angst, and J. Hemberger, "Dielectric properties of charge-ordered $LuFe_2O_4$ revisited: the apparent influence of contacts," Physical Review Letters **109**, 016405 (2012).
30. A. Ruff, S. Krohns, F. Schrettle, V. Tsurkan, P. Lunkenheimer, and A. Loidl, "Absence of polar order in $LuFe_2O_4$," The European Physical Journal B **85**, 1–6 (2012).
31. S. Lafuerza, J. García, G. Subías, J. Blasco, K. Conder, and E. Pomjakushina, "Intrinsic electrical properties of $LuFe_2O_4$," Physical Review B **88**, 085130 (2013).
32. T. Nagata, P.-E. Janolin, M. Fukunaga, B. Roman, K. Fujiwara, H. Kimura, J.-M. Kiat, and N. Ikeda, "Electric spontaneous polarization in $YbFe_2O_4$," Applied Physics Letters **110**, 052901 (2017).
33. K. Fujiwara, Y. Fukada, Y. Okuda, R. Seimiya, N. Ikeda, K. Yokoyama, H. Yu, S. Koshihara, and Y. Okimoto, "Direct evidence of electronic ferroelectricity in $YbFe_2O_4$ using neutron diffraction and nonlinear spectroscopy," Scientific Reports **11**, 1–7 (2021).
34. T. Fujii, N. Okamura, H. Hashimoto, M. Nakanishi, J. Kano, and N. Ikeda, "Structural, magnetic and optical properties of $YbFe_2O_4$ films deposited by spin coating," AIP Advances **6**, 085213 (2016).
35. R. Kashimoto, T. Yoshimura, A. Ashida, and N. Fujimura, "Lowering the growth temperature of strongly-correlated $YbFe_2O_4$ thin films prepared by pulsed laser deposition," Thin Solid Films **614**, 44–46 (2016), 9th International Symposium on Transparent Oxide and Related Materials for Electronics and Optics (TOEO9).
36. T. Nagata, K. Hiraoka, T. Okamoto, and N. Iwata, "Crystal structure of $YbFe_2O_4$ films prepared under different partial oxygen pressure," Thin Solid Films **665**, 96–98 (2018).
37. K. Shimamoto, J. Tanaka, K. Miura, D. Kiriya, T. Yoshimura, and N. Fujimura, "Change in the defect structure of composition controlled single-phase $YbFe_2O_4$ epitaxial thin films," Japanese Journal of Applied Physics **59**, SPPB07 (2020).
38. R. Rai, J. Hinz, M. Pascolini, F. Sun, and H. Zeng, "Electronic excitations and optical properties of $YbFe_2O_4$ thin films," Thin Solid Films **673**, 57–61 (2019).
39. F. Padera, "Measuring absorptance (k) and refractive index (n) of thin films with the perkinelmer lambda 950/1050 high performance uv-vis/nir spectrometers," Spectrometers Application Note: UV/Vis Spectroscopy (2013).
40. Y. Hishikawa, N. Nakamura, S. Tsuda, S. Nakano, Y. Kishi, and Y. Kuwano, "Interference-free determination of the optical absorption coefficient and the optical gap of amorphous silicon thin films," Japanese Journal of Applied Physics **30**, 1008 (1991).
41. R. Swanepoel, "Determination of the thickness and optical constants of amorphous silicon," Journal of Physics E: Scientific Instruments **16**, 1214 (1983).
42. R. Rai, A. Delmont, A. Sprow, B. Cai, and M. Nakarmi, "Spin-charge-orbital coupling in multiferroic $LuFe_2O_4$ thin films," Applied Physics Letters **100**, 212904 (2012).
43. R. Rai, J. Hinz, G. Petronilo, F. Sun, H. Zeng, M. L. Nakarmi, and P. Niraula, "Signature of structural distortion in optical spectra of YFe_2O_4 thin film," AIP Advances **6**, 025021 (2016).
44. K. Kuepper, M. Raekers, C. Taubitz, M. Prinz, C. Derks, M. Neumann, A. Postnikov, F. De Groot, C. Piamonteze, D. Prabhakaran, *et al.*, "Charge order, enhanced orbital moment, and absence of magnetic frustration in layered multiferroic $LuFe_2O_4$," Physical Review B **80**, 220409 (2009).
45. H. Xiang and M.-H. Whangbo, "Charge order and the origin of giant magnetocapacitance in $LuFe_2O_4$," Physical Review Letters **98**, 246403 (2007).
46. X. Xu, J. De Groot, Q.-C. Sun, B. C. Sales, D. Mandrus, M. Angst, A. Litvinchuk, and J. Musfeldt, "Lattice dynamical probe of charge order and antipolar bilayer stacking in $LuFe_2O_4$," Physical Review B **82**, 014304 (2010).
47. J. Pankove, "Optical processes on semiconductors," Dover Publications, New York (1971).